Development of a Novel 18F-labeled Probe for PET imaging of Estrogen Receptor β

Yujing Zhou (zhouyujing0402@163.com)
Qilu Hospital of Shandong University

Peng Lei
Shanghai Institute of Materia Medica Chinese Academy of Sciences

Jiaxin Han
Nanjing University of Chinese Medicine

Zhiming Wang
Shanghai Institute of Materia Medica Chinese Academy of Sciences

Aiyan Ji
Shanghai Institute of Materia Medica Chinese Academy of Sciences

Yuyang Wu
Shanghai Institute of Materia Medica Chinese Academy of Sciences

Lingling Zheng
Huashan Hospital Fudan University

Xiaoqing Zhang
Huashan Hospital Fudan University

Chunrong Qu
Shanghai Institute of Materia Medica Chinese Academy of Sciences

Jian Min
Hubei University

Weiliang Zhu
Shanghai Institute of Materia Medica Chinese Academy of Sciences

Zhijian Xu
Shanghai Institute of Materia Medica Chinese Academy of Sciences

Xingdang Liu
Huashan Hospital Fudan University

Hao Chen
Shanghai Institute of Materia Medica Chinese Academy of Sciences

Zhen Cheng
Shanghai Institute of Materia Medica Chinese Academy of Sciences https://orcid.org/0000-0001-8177-9463

Research Article

Keywords: Estrogen receptor β, 18F, Positron emission tomography, Nuclear receptor

Posted Date: February 15th, 2022

DOI: https://doi.org/10.21203/rs.3.rs-1334238/v1

Abstract

Purpose: Estrogen receptors beta (ERβ) is an important ER subtype and plays crucial roles in many physiological and pathological disorders. Herein, we aim to develop a probe, ^{18}F-PVBO, for *in vivo* ERβ targeted PET imaging with promising results.

Methods: ^{18}F-PVBO was synthesized using a two-step radiolabeling method. The relative binding affinities of the reference compound PVBO towards ERα and ERβ were determined by a competitive radiometric binding assay using ^{3}H-estradiol. Cytotoxicity and cell uptake were evaluated in ERβ-positive DU145 cells. PET imaging, including blocking study, was performed in DU145 tumor-bearing nude mice (n = 3 per group), and the biodistribution study of ^{18}F-PVBO was also performed.

Results: The non-radioactive PVBO showed 12.46-fold stronger binding affinity to ERβ than to ERα *in vitro*. ^{18}F-PVBO was synthesized with a 15-28% radiochemical yield (n = 5) within 40 min, and the radiochemical purity was >98%. The uptake of ^{18}F-PVBO in DU145 cells was significantly blocked by ERB-041 ($p < 0.05$). The uptake of ^{18}F-PVBO in DU145 xenografts increased during the 120 min dynamic scanning, with a maximum uptake of 2.80 ± 0.30% ID/g at 120 min. Based on time active curves (TACs), injection of ^{18}F-PVBO with unlabeled PVBO or ERB-041 resulted in a significant signals reduction with the T/M ratio <1 at 30, 60, 75, and 120 min post-injection (p <0.05). Comparison of the %ID/g showed ^{18}F-PVBO had a higher T/M ratio compared to ^{18}F-FES in DU145 tumor-bearing mice at 60 min (1.65 *vs.* 1.28), 75 min (1.76 *vs.* 1.35), and 120 min (1.80 *vs.* 1.37) ($p < 0.05$).

Conclusion: ^{18}F-PVBO shows 12.46-fold stronger binding to ERβ over ERα, with high radiochemical stability. It demonstrates the feasibility of noninvasively imaging ERβ positive tumors by small-animal PET and provides a new strategy for visualizing of ERβ *in vivo*.

Introduction

For decades, molecular imaging has brought significant impact to clinical diagnosis and treatment strategies. Functional receptors are the primary theranostic targets in nuclear medicine and have been actively investigated for targeted imaging and therapy in preclinical research and clinical practice. It is well established that estrogen receptor (ER), function as an essential nuclear receptor, is a valuable biomarker for noninvasive imaging of hormonal status[1]. ERα is the most widely studied ER at present[2]. Evidence proves the significance of ERα in determining the diagnosis and treatment of patients with estrogen-dependent cancers[3, 4]. Notably, ERα was regarded as the only ER form until ERβ was firstly cloned in 1996[2]. ERβ has a DNA-binding domain and ligand-binding domain that is 96% and 60% homologous with those of ERα, respectively[2], indicating that it may have similar but not identical functions. In addition to presenting in mammary epithelial and ductal cells, ERβ is detected in various tissues, such as subcutaneous adipose tissue[5], brain, and prostate[6]. Furthermore, changes in ERβ expression levels and downstream pathways are involved in regulating many physiological and pathological processes[7–9], such as the occurrence and development of the Parkinson's disease[10],

endometriosis[11], coronary heart disease[12], and diabetes[13]. All these findings highlight ERβ to be a promising biomarker for the early diagnosis of a variety of diseases.

With more evidence showing different functions of ERα and ERβ, independent imaging and quantification of them using molecular imaging technique are desired for defining their roles in living subjects. The food drug administration (FDA) - approved positron emission tomography (PET) probe, 16α-^{18}F-17β-fluoroestradiol (^{18}F-FES), for ER targeting shows 6.3 times binding affinity for ERα than that of ERβ[14]. It has been recognized as an ERα specific PET probe[15] and widely used to screen and evaluate breast cancer patients receiving endocrine therapy[16]. Given its much higher binding to ERα and relatively narrow indications, ^{18}F-FES has limitations in the molecular imaging of ERβ and ERβ related diseases.

At present, applications for ERβ PET imaging have been rarely studied. Some attempts have been spent to develop ERβ PET probes, while all the results are disappointing. For example, Yoo J. *et al.* developed ^{18}F-FEDNP, which has an 8.3-fold binding affinity preference for ERβ over ERα. Biodistribution studies were performed in the ER knockout mice, but the probe's specific uptake levels were modest[17]. Lee J. K. *et al.* reported ^{18}F-8BFEE$_2$ with high ERβ selectivity, but the attempts to improve in vivo targeting ability and biodistribution profile failed[18]. Antunes I. F. *et al.* reported ^{18}F-FHNP had 3.5 times higher binding affinity for ERβ over ERα. The PET imaging was performed in ERα positive SKOV3 xenograft model, and ^{18}F-FHNP showed 2-fold lower tumor uptake than ^{18}F-FES[19]. The previous studies highlight the strong need to develop new generation PET probes for evaluating ERβ levels *in vivo*.

Previously, a series of diphenolic azoles were studied as highly selective ERβ agonists. The 7-position-substituted benzoxazoles were reported to have high ERβ binding selectivity. Among them, 2-(3-fluoro-4-hydroxyphenyl)-7-vinyl-1,3-benzoxazol-5-ol (ERB-041) was reported to have the best selectivity (255.5-fold higher selectivity for ERβ over ERα)[20]. Herein, inspired by the above study, we developed a ^{18}F-labeled small molecule PET probe based on ERB-041, ^{18}F-2-(3-(2-(2-(2-fluoroethoxy)ethoxy)ethoxy)-4-hydroxyphenyl)-4-vinylbenzo[d]oxazol-6-ol (^{18}F-PVBO, Scheme 1), for ERβ imaging with a 12.46-fold higher selectivity over ERα. After getting satisfactory *in vitro* relative binding affinities of PVBO, ^{18}F-PVBO was synthesized in high radiochemical yield and purity. The *in vitro* cell uptake in DU145 cells and *in vivo* DU145 xenografts PET/CT imaging and blocking experiment confirmed specific ERβ targeting ability of ^{18}F-PVBO. In summary, by biological evaluation of ERβ-targeted PET probe, it has been found that ^{18}F-PVBO performs as a specific targeting PET probe for ERβ *in vivo* imaging. Our finding provides a promising method for noninvasive imaging of ERβ.

Material And Methods

Chemistry-General Methods

All of the reagents and materials were purchased from Sigma Chemical Co. (St. Louis, MO, USA), Bide Pharmatech Co. (Shanghai, China), and Energy Chemical Co. (Shanghai, China). Reactions took place

opening to the atmosphere unless otherwise specified. The reactions were monitored by thin-layer chromatography (TLC) using 200 μM silica gel (China National Pharmaceutical Group Co., China) or Dionex UltiMate 3000 HPLC. ^{1}H and ^{13}C NMR spectra were recorded on a Bruker Avance III 400 spectrometer. High-resolution mass spectra (HRMS) were performed on an Agilent G6520 Q-TOF mass spectrometer. ^{18}F-Fluoride was produced using a Sumitomo 10MeV cyclotron. ^{18}F-Fluoride was produced from ^{18}O-water and the $^{18}O(p,n)^{18}F$ reaction. The synthesis and characterization of PVBO and the precursor are presented in supplemental materials.

In vitro relative binding affinity of the reference compound PVBO towards ERα and ERβ

Relative binding affinities were determined by a competitive radiometric binding assay using ^{3}H-estradiol ([2,4,6,7-^{3}H]-17β-estradiol, 70-115 Ci/mmol, Perkin-Elmer, Waltham, MA). Data are presented as the relative binding affinity (RBA) with the RBA of estradiol towards ERα and ERβ set to 100%. The experiment and data analysis were performed according to a previously described binding assay protocol[21].

Computational Details

Molecular docking for PVBO was performed against ERα using the highest resolution X-ray crystal structure (PDB entry 6VIG, 1.45 Å) by Schrodinger suit[22]. As for ERβ, molecular docking was performed with the crystal structure of ERβ complexed with ERB-041 (2-(3-fluoro-4-hydroxyphenyl)-7-vinyl-1,3-benzoxazol-5-ol) (PDB entry 1X7B), because PVBO was derived from ERB-041. All the water molecules as well as the ligand were removed by PyMOL. Before docking, the Schrödinger protein preparation wizard module was used to prepare the 3D structures of protein, optimize 3D structures with pH = 7.0, and restrain minimization converge heavy atoms to RMSD of 0.30 Å, using force field OPLS_2005. The docking grid of 20 Å was generated over the co-crystallized ligand with the Receptor grid generation module. PVBO and ERB-041 were pre-processed by the Ligprep, with Epik to generate the proper protonation states at pH 7.0, with at most 32 stereoisomers generated. The compounds were then docked to the protein using the “extra precision” glide docking.

Radiosynthesis

Starting from unlabeled precursor 12, ^{18}F-PVBO was obtained using a two-step radiosynthetic method. The ^{18}F-fluoride solution was passed through a QMA SepPak Light anion exchange cartridge (Waters) and eluted from the cartridge into a vial with MeCN (aq) (1.1 ml) containing Krypotofix 222 (13 mg) and K_2CO_3 (3 mg). The solvents were evaporated at 120 °C and then dried 3 more times by adding 1 ml of MeCN. Then, precursor 12 was dissolved in 1 ml of MeCN and added to the vial. The reaction system was

sealed and heated at 120 °C for 20 min. After the solvents were evaporated, 1 ml of DCM and 0.25 ml of TFA were added, and the mixture was heated at 60 °C for 5 min to remove the methoxymethyl ether group. The product was purified by HPLC (Column: XBridge BEH C18 OBD Prep Column, 5 μm, 10 mm × 250 mm; eluent: acetonitrile in 0.3% phosphoric acid solution; flow: 3 ml/min.^{18}F-FES was produced as previously described[23].

Distribution coefficients (Log $D_{7.4}$)

HPLC-purified ^{18}F-PVBO (100 μCi/tube) was added to a mixture of n-octanol/PBS pH 7.4 (0.5 mL/0.5 mL). After vortexing at room temperature for 10 min, the tubes were shaken in a water bath at 37°C for 30 min. After standing for stratification, 0.2 mL of solution was drawn from both phases. The radioactivity was counted using an automated gamma counter (Wizard 2, model 2480, PerkinElmer). The experiments were performed in triplicate.

In vitro stability

The stability of ^{18}F-PVBO was measured in PBS or fetal bovine serum (FBS). Briefly, ^{18}F-PVBO (100 μL, 37 MBq/mL) was added to 500 μL of PBS or FBS and incubated at 37 °C for 1 h or 2 h. Stability was evaluated by HPLC.

Cell culture and animal models

The human prostate cancer cell line DU-145 and the mouse embryonic fibroblast cell line NIH/3T3 were purchased from the American Type Culture Collection (Manassas, USA). Cells were cultured in the Minimum Essential Medium (MEM, Gibco, Carlsbad, USA) or Dulbecco's modified Eagle's medium (DMEM, Gibco, Carlsbad, USA) supplemented with 10% FBS (Gibco, Carlsbad, USA) in a 37°C incubator with 5% CO_2.

Athymic female nude mice (6-8 weeks, n = 10, Slaccas, Shanghai, China) and female BALB/c mice (10-12 weeks, n = 15, Slaccas, Shanghai, China) were used in this study. All animal experiments were approved by the Institutional Animal Care and Use Committee of the Shanghai Institute of Materia Medica, Chinese Academy of Sciences. After one week of acclimatization, DU-145 cells (1 ×10^6 cells/mouse) were injected into the right thigh subcutaneously.

Cytotoxicity assay

The DU-145 cell line and NIH/3T3 cell line were cultured in MEM or DMEM supplemented with 10% FBS in a 37°C incubator with 5% CO_2. MTT was used to assess the cytotoxicity of different concentrations (0, 10,

25, 50, 75, and 100 μM) of the unlabeled PVBO on these two cell lines. Briefly, 100 μL of cells were seeded in a 96-well plate at a cell density of 5000 cells/well and incubated for 24 h. The cells were treated with PVBO at different concentrations (0, 10, 25, 50, 75, and 100 μM) and incubated for 24 h. Ten microliters of MTT solution were added to each well and incubated for another 4 h. Then, the MTT solution was discarded, 150 μL of DMSO was added to each well, and the absorbance at 490 nm was measured with a microplate reader (Synergy H1 Hybrid, Biotek, Winooski, USA).

Cell uptake

Cell uptake was performed using DU145 cells in the presence and absence of the ERβ selective drug ERB-041[20]. DU145 cells were seeded in 12-well plates at a cell density of 1×10^5 cells/well and incubated for 24 h. Fresh serum-free medium (1 ml) containing ^{18}F-PVBO (37 MBq) was added to each well. To inhibit the uptake of ^{18}F-PVBO, DU145 cells were pretreated with the ERβ-selective ERB-041 for 1 h and then incubated with ^{18}F-PVBO (37 MBq) at 37°C for 15, 30, 60, and 120 min. Each well was washed with PBS three times before cell lysis with NaOH. The results were measured using an automatic gamma counter (Wizard 2, model 2480, PerkinElmer). Cell uptake is presented as the percentage of the total added radioactivity dose.

Immunohistochemical (IHC) staining

DU145 tumors were fixed with formalin. IHC staining was performed on 4 μm sections taken from paraffin-embedded tumor tissues. After rehydration, the sections were incubated with a 1:200 dilution of the primary antibody, rabbit anti-estrogen receptor alpha antibody (ab3575, Abcam, Cambridge, UK) and rabbit anti-estrogen receptor β antibody (ab3576, Abcam, Cambridge, UK) at 4°C overnight. Then, the sections were incubated with a biotinylated secondary antibody (ab205718, Abcam, Cambridge, UK) and treated with Avidin-biotin-peroxidase. The 3-amino-9-ethylcarbazole substrate chromogen was used, followed by tissue counterstaining with hematoxylin. Sections were examined and photographed using a confocal microscope (Olympus, Tokyo, Japan)

Western blot

The membranes were incubated with 1:1000 dilutions of primary rabbit anti-estrogen receptor alpha (ab3575, Abcam, Cambridge, UK), rabbit anti-estrogen receptor β (ab3576, Abcam, Cambridge, UK) and anti-GAPDH (1:50000, 60004-1-Ig, Proteintech, Rosemont, USA) antibodies at 4 °C overnight. The next day, after washing with PBS three times for 10 min each, the membranes were incubated with the secondary antibodies for 1 h at room temperature. Finally, the target proteins were visualized using a LAS4000 enhanced chemiluminescence system (GE Healthcare, Wisconsin, USA).

Micro-PET/CT

Micro-PET/CT (Inveon, Siemens Company, Germany) studies were carried out in DU145-bearing athymic female nude mice using ^{18}F-PVBO or ^{18}F-FES. The *in vivo* targeting specificity of ^{18}F-PVBO was evaluated in a blocking study with the administration of unlabeled PVBO (5 μmol/kg) or ERB-041 (5 μmol/kg) 30 min before ^{18}F-PVBO injection. The dose of ^{18}F-PVBO was 7.02 ± 0.93 MBq per mouse. The dose of ^{18}F-FES was 6.51 ± 0.64 MBq per mouse. A 120 min dynamic PET scan was immediately performed for 2 h after injecting the radiotracer through the tail vein. A 10 min CT scan was acquired for anatomic localization. The relative position of the organ was defined based on the anatomy of CT. The uptake values were expressed as the percentage of the injected dose per gram of tissue (%ID/g).

Biodistribution

BALB/c mice were anesthetized via inhalation of 2% isoflurane and injected with 3-5 MBq radiotracer through the tail vein for the biodistribution study. The mice were sacrificed at 30 min, 60 min and 120 min after injection. Blood was withdrawn by cardiac puncture, and the organs/tissues were collected, weighed and evaluated using an automatic gamma counter (Wizard 2, model 2480, PerkinElmer). Uptake values were expressed as percentage of injected dose per gram (%ID/g).

Histological analysis of major organs

The mice were sacrificed at 7 days after ^{18}F-PVBO PET imaging. Tissue samples from the heart, liver, spleen, lung, kidney, and brain were collected for pathological examination. H&E staining of the major organs of nude mice was performed based on a standard procedure[24].

Statistical analysis

GraphPad Prism 5 (GraphPad Software, CA, USA) and SPSS 24.0 software (SPSS, Inc., Chicago, IL) were used for statistical analyses. The data are expressed as the mean ± standard deviation (SD). Differences between groups were analyzed using a two-sided unpaired Student's *t*-test. Differences were considered statistically significant at $p < 0.05$ (*$p < 0.05$; ** $p < 0.01$; *** $p < 0.001$).

Results

Probe synthesis

The tosylate-precursor compound 12 for radiofluorination and the non-radioactive reference compound PVBO were obtained by multiple organic synthesis steps including MOMBr and TBSCl hydroxyl group protection, nitration reaction, Wittig reaction, reduction reaction, aldoamine condensation, and fluorination

reaction (Fig. 1). The products were characterized and confirmed by mass spectroscopy (MS) and nuclear magnetic resonance (NMR), including ^{1}H-NMR and ^{13}C-NMR as listed in the experimental section. The purification of the compounds was performed by Semi-Preparative HPLC. The purity of the product was above 98%.

Radiochemistry and stability of ^{18}F-PVBO

Starting from unlabeled precursor 12, ^{18}F-PVBO was obtained using a two-step radiosynthetic method (Fig. 2a). The product was purified by HPLC (retention time of unlabeled PVBO = 13.91 min; retention time of ^{18}F-PVBO = 14.14 min). ^{18}F-PVBO was synthesized with a 15-28% radiochemical yield within 40 min (n = 5), and the radiochemical purity was higher than 98% (Fig. 2b). The specific activity was 7.5 GBq/μmol. The partition coefficient (Log$D_{7.4}$) was 0.96 ± 0.03.

HPLC analysis showed no other peaks after incubating ^{18}F-PVBO in PBS or FBS for up to 2 h (Fig. 2c), indicating that the probe maintained high stability under physiological conditions.

In vitro binding affinity and cytotoxicity

The relative binding affinity (RBA) of the reference compound PVBO for ERα and ERβ was 0.52% and 6.48% relative to estradiol, respectively. PVBO showed a 12.46-fold higher selectivity for ERβ than for ERα. Cell viability was found to be over 90% after treatment with PVBO at concentrations as high as 100 μM, suggesting PVBO displayed low cytotoxicity towards DU145 cells and NIH/3T3 cells (Supporting fig. S1).

Molecular docking study

The docking score of PVBO against ERα (Fig. 3a) was -8.11 Kcal/mol, weaker than that of ERβ (Fig. 3b), -8.25 Kcal/mol, which was in consistent with the relative binding affinity data. Docking of ERB-041 against its own crystal structure receptor (self-docking) yielded the docking score of -8.30 Kcal/mol with the binding mode comparatively consistent with the crystal conformation (RMSD = 0.33) (Fig. 3c).

ERβ expression in DU145 cells and cell uptake of ^{18}F-PVBO

The results of IHC showed that in DU145 xenografts, the expression of ERα was barely detectable, while the expression of ERβ was much higher (Supporting fig. S2). Western blotting results showed that compared with NIH/3T3 cells, DU145 cells had a significantly higher ERβ expression (Fig. 4a). The uptake of ^{18}F-PVBO in DU145 cells increased with extending incubation times and reached 4.17±0.29% after 120 min. Importantly, in the presence of ERB-041, there was significant inhibition uptake of ^{18}F-PVBO at 15, 30, 60, and 120 min (Fig. 4b, $p < 0.05$).

Micro-PET/CT *in vivo* imaging

Representative PET/CT images of ^{18}F-PVBO and ^{18}F-FES in DU145 tumor-bearing mice are shown in Fig. 5a and 5b. Based on the time activity curves (TACs) of ^{18}F-PVBO, the tumor uptake showed a gradual upward trend over 120 min dynamic scan (Fig. 5d, n = 3). The maximum uptake was 2.80 ± 0.30% ID/g at 120 min. All images also showed high liver uptake along with intestinal excretion. As a comparison, ^{18}F-FES showed maximum accumulation in the tumor at 10 min post-injection (PI), with a gradual decrease during 120 min of scanning (1.80 ± 0.13% ID/g at 120 min) (Fig. 5e, n = 3). As shown in Fig. 5c, in the pre-injected PVBO and ERB-041 groups, only weak tumor signals were recorded in PET images at 120 min. The TACs of the blocking experiment are shown in Fig. 5f and 5g (n = 3 per group). Based on the T/M ratio, co-injection of ^{18}F-PVBO with unlabeled PVBO or ERB-041 resulted in a significant reduction of the T/M ratio at each time point ($p < 0.05$). Importantly, T/M ratios of ^{18}F-PVBO were higher than ^{18}F-FES in DU145 tumor-bearing mice at 60 min (1.65 *vs.* 1.28), 75 min (1.76 *vs.* 1.35), and 120 min (1.80 *vs.* 1.37) PI (Fig. 5h, $p < 0.05$).

Biodistribution of ^{18}F-PVBO

To further evaluate the *in vivo* characteristics of ^{18}F-PVBO, a biodistribution experiment was performed in BALB/c mice. ^{18}F-PVBO showed high accumulation in the liver and heart, with a slow clearance in 120 min. The liver uptake was 21.21 ± 9.79% ID/g at 30 min PI and decreased to 14.02 ± 8.65% ID/g at 120 min PI. The uptake of the small intestine was 2.00 ± 0.89% ID/g at 30 min and increased to 12.02 ± 11.86% ID/g at 60 min PI, indicating clearance of ^{18}F-PVBO through the liver-hepatobiliary system. The radioactive signals of the kidney and bladder were at a low level. Accumulation of ^{18}F-PVBO in the brain was observed. Uptake in bone was found and reached 6.01 ± 4.58% ID/g at 120 min PI, indicating moderate defluorination of ^{18}F-PVBO in mice (Fig. 6, Supporting table S1).

H&E staining

The mice were sacrificed 7 days after ^{18}F-PVBO PET imaging. Tissue samples from the heart, liver, spleen, lung, kidney, and brain were collected for pathological examination. Based on H&E staining, no acute pathological changes were observed in these tissues (Supporting fig. S3).

Discussion

The discovery of PET was a milestone in the development of modern imaging technology. At present, it is a highly powerful imaging method to detect cellular and molecular events *in vivo*, which reveals metabolic function through uptake of the radionuclide-labeled probe[25]. Although research on hormone ligands in nuclear medicine is in the ascendant, ERβ-targeted radioactive probes are not intensively investigated. Meanwhile, because of limited pathological information of ERβ, the choice of animal

models for PET imaging of ERβ is difficult. Researchers even performed *in vivo* ERβ PET imaging using ERα positive SKOV3 xenograft model, but the result was not satisfactory because of the high expression of ERα in SKOV3 cells[19]. Similarly, the previously reported PET probe ^{18}F-FEDNP tested in ER knockout mice, was regarded as not suitable for ERβ PET imaging[17]. Another study introduced ^{18}F-8BFEE$_2$ to achieve good ERβ selectivity, it did not conduct further *in vivo* imaging[18]. To the best of our knowledge, no *in vivo* imaging study using ERβ positive model has been carried out, although some ligands have been reported to possess good ERβ selectivity[18]. DU145 cells were reported to express only ERβ[26, 27], and in our study, ERβ expression was verified by western blot and immunohistochemistry, implying DU145 xenografts can be used a model for ERβ PET imaging.

The goal of our work is to develop an ^{18}F-labeled probe to enable noninvasive imaging of ERβ expression in living tissues. Based on previous research, the 7-position-substituted benzoxazoles attracted our attention[20]. Although Zhou *et al.* successfully converted the 7-position-substituted benzoxazoles compound **92** into ERβ selective probe through radiobromination, there was no further cell tests and *in vivo* PET imaging to investigate the performance of the probe[28]. In our study, before the radiosynthesis, a competitive radiometric binding assay was performed using ^{3}H-estradiol, revealing a 12.46-fold higher selectivity of PVBO for ERβ over ERα. This value is lower than the reported value for ERB-041 (255.5-fold higher selectivity for ERβ)[29]. To gain insight into the binding nature of PVBO to ERβ, molecular docking simulations were performed. The docking score of PVBO against ERβ is worse than that of ERB-041, -8.25 Kcal/mol *vs.* -8.30 Kcal/mol, suggesting that the chemical modification of 7-position-substituted of benzoxazoles decreases the ERβ selectivity. Although PVBO adopts a similar binding mode to ERB-041 against ERβ regarding the ERB-041 part, the extended side chain of PVBO abolishes the hydrogen bond between Arg-346 in the ERβ and phenolic hydroxyl in the PVBO. Meanwhile, no significant cytotoxicity was found at a concentration as high as 100 μM, inspiring us to carry further radiolabeling and cell uptake studies.

^{18}F-PVBO was successfully prepared by two-step radiosynthetic method based on the precursor 12. ^{18}F-PVBO meets the requirements of PET/CT imaging as its high radiochemical purity, specific activity, high stability and low cytotoxicity. The uptake of ^{18}F-PVBO in DU145 cells increased with extending incubation times due to their ERβ expression and could be significantly blocked by ERB-041, demonstrating the ERβ binding specificity of ^{18}F-PVBO.

Inspired by the specific ERβ binding ability of ^{18}F-PVBO, we further explored its PET imaging performance in DU145 tumor-bearing nude mice models. *In vivo* PET imaging successfully visualized ERβ positive DU145 xenograft tumors in mice models. The uptake of ^{18}F-PVBO gradually accumulated in the tumor during dynamic scanning. Co-administration of PVBO or ERB-041 reduced tumor uptake at 2h PI by approximated 50% and 75%, respectively, demonstrating the ERβ targeting specificity of ^{18}F-PVBO. ^{18}F-FES possessed 2.5-fold higher selectivity for ERα and was considered to provide accurate information about ER expression[30]. In our study, at 2h PI, a 1.3-fold higher T/M ratio was observed of ^{18}F-PVBO than ^{18}F-FES, indicating that ^{18}F-PVBO provides better tumor visualization ability for monitoring ERβ-positive

tumors. Collectively, the *in vitro* and *in vivo* results showed that ^{18}F-PVBO can be used to image ERβ positive tumors.

To further clarify the distribution of ^{18}F-PVBO, a biodistribution study was performed using BALC/c mice. After injection of ^{18}F-PVBO, the radioactive signal in the blood reached a high level at 30 min and then decreased rapidly at 60 and 120 min. The uptake in the bone was detected 30 min PI and reached a moderate level at 60 min PI, suggesting that ^{18}F-PVBO was defluorinated *in vivo*[31], which may be related to the liver metabolism[30, 32]. Interestingly, it has been found that the bone uptake of ^{18}F-labeled probes in mice is much higher than in primates[33]. Whether ^{18}F-PVBO will be seriously defluorinated in primates needs further investigation.

Our study meets the urgent needs of noninvasive ERβ detection in living systems. Significant uptake and slow clearance were observed in the heart, which confirmed its future application in ERβ-related heart disease. The imaging data also showed that ^{18}F-PVBO passed the blood-brain barrier, implying ^{18}F-PVBO may provide an advantage for the diagnosis of ERβ-related intracranial diseases. Because of the lack of *in vivo* ERβ quantification method, research on the gradual change of ERβ in different disease models is complicated. ^{18}F-PVBO has the potential to change such situation.

Conclusion

A novel ^{18}F-labeled small molecule, ^{18}F-PVBO, has been developed for PET imaging of ERβ expression. The probe shows 12.46-fold stronger binding to ERβ over ERα, with high radiochemical stability and low cytotoxicity. ^{18}F-PVBO demonstrates the feasibility of noninvasively imaging ERβ positive tumors by small-animal PET. It may provide a new strategy for visualizing ERβ *in vivo*. Molecular imaging with PET/CT using ERβ-specific PET probes is expected to help understand the roles of ERβ in various diseases and facilitate the detection of ERβ in clinical setting.

Declarations

Funding

This work was partially supported by the National Key Research and Development Program of China 2021YFC2100300 (JM), the National Natural Science Foundation of China under Grant No. 82071976 (HC) and 81901799 (CQ), Shanghai Pujiang Program (19PJ1411100) (HC), and Shanghai Municipal Science and Technology Major Project (HC, ZC), National Key Research and Development Plan Digital Diagnosis and Treatment Equipment Research and Development Project (2017YFC0113300) (XL) and Pudong Hospital, Fudan University, college project (YJYJRC202108/ YJYJRC202101/Zdzk2020-14) (XL). The authors wish to thank Haibing Zhou (School of Pharmaceutical sciences, Wuhan university) to provide ERβ protein. We thank Sheng Liang (Department of nuclear medicine, Xinhua hospital, Shanghai

jiao tong university) and Shaoli Song (Department of nuclear medicine, Shanghai cancer center, Fudan University) for technical assistance in radiosynthesis of PET probes.

Data availability

The datasets generated during and/or analysed during the current study are available from the corresponding author on reasonable request.

Code availability

Not applicable.

Author contribution

All authors contributed to the study conception and design. Material preparation, data collection and analysis were performed by Yujing Zhou, Peng Lei, Jiaxin Han, Zhiming Wang, Aiyan Ji, Yuyang Wu, Lingling Zheng and Xiaoqing Zhang. The first draft of the manuscript was written by Yujing Zhou, Peng Lei, Jiaxin Han and Zhiming Wang. The review and editing of the manuscript was completed by Jian Min, Weiliang Zhu, Zhijian Xu, Hao Chen and Zhen Cheng. Fundings were obtained by Chunrong Qu, Jian Min, Xingdang Liu, Hao Chen and Zhen Cheng. All authors commented on previous versions of the manuscript. All authors read and approved the final manuscript.

Ethics approval

Approval was obtained from the Institutional Animal Care and Use Committee of the Shanghai Institute of Materia Medica, Chinese Academy of Sciences.

Consent for publication

Not applicable.

Consent for interest

The authors have no relevant financial or non-financial interests to disclose.

References

1. Pearce, S. T.; Jordan, V. C., The biological role of estrogen receptors alpha and beta in cancer. Critical Reviews in Oncology Hematology. 2004; 50 (1): 3-22.
2. Kuiper, G.; Enmark, E.; PeltoHuikko, M., et al., Cloning of a novel estrogen receptor expressed in rat prostate and ovary. Proc Natl Acad Sci U S A. 1996; 93 (12): 5925-5930.
3. Nilsson, S.; Makela, S.; Treuter, E., et al., Mechanisms of estrogen action. Physiol Rev. 2001; 81 (4): 1535-65.
4. Kumar, M.; Salem, K.; Michel, C., et al., (18)F-fluoroestradiol PET imaging of activating estrogen receptor-alpha mutations in breast cancer. J Nucl Med. 2019; 60 (9): 1247-1252.
5. Crandall, D. L.; Busler, D. E.; Novak, T. J., et al., Identification of estrogen receptor beta RNA in human breast and abdominal subcutaneous adipose tissue. Biochem Biophys Res Commun. 1998; 248 (3): 523-6.
6. Kuiper, G. G.; Shughrue, P. J.; Merchenthaler, I., et al., The estrogen receptor beta subtype: a novel mediator of estrogen action in neuroendocrine systems. Front Neuroendocrinol. 1998; 19 (4): 253-86.
7. Balla, B.; Sarvari, M.; Kosa, J. P., et al., Long-term selective estrogen receptor-beta agonist treatment modulates gene expression in bone and bone marrow of ovariectomized rats. J Steroid Biochem Mol Biol. 2019; 4 (188): 185-194.
8. Liu, J. Y. H.; Lin, G.; Fang, M. R., et al., Localization of estrogen receptor ER alpha, ER beta and GPR30 on myenteric neurons of the gastrointestinal tract and their role in motility. Gen Comp Endocrinol. 2019; 1 (272): 63-75.
9. Le Moene, O.; Stavarache, M.; Ogawa, S., et al., Estrogen receptors alpha and beta in the central amygdala and the ventromedial nucleus of the hypothalamus: Sociosexual behaviors, fear and arousal in female rats during emotionally challenging events. Behav Brain Res. 2019; 23 (367): 128-142.
10. Kim, H.; Park, J.; Leem, H., et al., Rhododendrin-induced RNF146 expression via estrogen receptor beta activation is cytoprotective against 6-OHDA-induced oxidative stress. Int J Mol Sci. 2019; 20 (7): e1772.
11. Han, S. J.; Jung, S. Y.; Wu, S. P., et al., Estrogen Receptor β Modulates Apoptosis Complexes and the Inflammasome to Drive the Pathogenesis of Endometriosis. Cell. 2015; 163 (4): 960-974.
12. Du, M.; Shan, J.; Feng, A., et al., Oestrogen receptor beta activation protects against myocardial infarction via Notch1 signalling. Cardiovasc Drugs Ther. 2020; 34 (2): 165-178.
13. Ofosu, W.; Mohamed, D.; Corcoran, O., et al., The role of oestrogen receptor beta (ERβ) in the aetiology and treatment of Type 2 diabetes mellitus. Curr Diabetes Rev. 2019; 15 (2): 100-104.
14. Kumar, P.; Mercer, J.; Doerkson, C., et al., Clinical production, stability studies and PET imaging with 16-alpha- 18F fluoroestradiol (18F FES) in ER positive breast cancer patients. J Pharm Pharm Sci. 2007; 10 (2): 256s-265s.
15. Kumar, M.; Salem, K.; Tevaarwerk, A. J., et al., Recent advances in imaging steroid hormone receptors in breast cancer. J Nucl Med. 2020; 61 (2): 172-176.

16. Kruchten, M. V.; Glaudemans, A. W. J. M.; Vries, E. F. J. D., et al., PET imaging of estrogen receptors as a diagnostic tool for breast cancer patients presenting with a clinical dilemma. J Nucl Med. 2012; 53 (2): 182-190.
17. Yoo, J.; Dence, C.; Sharp, T., et al., Synthesis of an estrogen receptor beta-selective radioligand: 5-[18F]fluoro-(2R,3S)-2,3-bis(4-hydroxyphenyl)pentanenitrile and comparison of in vivo distribution with 16alpha-[18F]fluoro-17beta-estradiol. J. Med. Chem. 2005; 48 (20): 6366-78.
18. Lee, J.; Peters, O.; Lehmann, L., et al., Synthesis and biological evaluation of two agents for imaging estrogen receptor β by positron emission tomography: challenges in PET imaging of a low abundance target. Nucl. Med Biol. 2012; 39 (8): 1105-16.
19. Antunes, I.; van Waarde, A.; Dierckx, R., et al., Synthesis and Evaluation of the Estrogen Receptor β-Selective Radioligand 2-F-Fluoro-6-(6-Hydroxynaphthalen-2-yl)Pyridin-3-ol: Comparison with 16α-F-Fluoro-17β-Estradiol. J. Nucl. Med. . 2017; 58 (4): 554-559.
20. Malamas, M. S.; Manas, E. S.; McDevitt, R. E., et al., Design and synthesis of aryl diphenolic azoles as potent and selective estrogen receptor-beta ligands. J Med Chem. 2004; 47 (21): 5021-5040.
21. Min, J.; Wang, P. C.; Srinivasan, S., et al., Thiophene-Core Estrogen Receptor Ligands Having Superagonist Activity. J Med Chem. 2013; 56 (8): 3346-3366.
22. Schrödinger Release 2020: Schrödinger, LLC, New York, NY. 2020.
23. Moresco, R.; Casati, R.; Lucignani, G., et al., Systemic and cerebral kinetics of 16 alpha [18F]fluoro-17 beta-estradiol: a ligand for the in vivo assessment of estrogen receptor binding parameters. J. Cerebr.Blood.F.Met. . 1995; 15 (2): 301-11.
24. Ye, S. Y.; Cui, C. X.; Cheng, X. J., et al., Red Light-Initiated Cross-Linking of NIR Probes to Cytoplasmic RNA: An Innovative Strategy for Prolonged Imaging and Unexpected Tumor Suppression. J Am Chem Soc. 2020; 142 (51): 21502-21512.
25. Terpogossian, M. M.; Phelps, M. E.; Hoffman, E. J., et al., Position emission transaxial tomograph for nuclear imaging(PETT). Radiology. 1975; 114 (1): 89-98.
26. Lau, K. M.; Laspina, M.; Long, J., et al., Expression of estrogen receptor (ER)-α and ER-β in normal and malignant prostatic epithelial cells: regulation by methylation and involvement in growth regulation. Cancer Res. 2000; 60 (12): 3175.
27. Ito, T.; Tachibana, M.; Yamamoto, S., et al., Expression of estrogen receptor (ER-alpha and ER-beta) mRNA in human prostate cancer. Eur Urol. 2001; 40 (5): 557-563.
28. Dong Zhou, H. Z., Carl C. Jenks, Jason S. Lewis, John A. Katzenellenbogen, and Michael J. Welch, Bromination from the macroscopic level to the tracer radiochemical level: (76)Br radiolabeling of aromatic compounds via electrophilic substitution. Bioconjugate Chem. 2009; 20 (4): 808-816.
29. Manas, E. S.; Unwalla, R. J.; Xu, Z. B., et al., Structure-based design of estrogen receptor-beta selective ligands. J Am Chem Soc. 2004; 126 (46): 15106-15119.
30. Yoo, J.; Dence, C. S.; Sharp, T. L., et al., Synthesis of an estrogen receptor beta-selective radioligand: 5- F-18 Fluoro-(2R*,3S*)-2,3-bis(4-hydroxyphenyl)pentanenitrile and comparison of in vivo distribution with 16 alpha- F-18 Fluoro-17 beta-estradiol. J Med Chem. 2005; 48 (20): 6366-6378.

31. V, F., Changes of fluoride content in bone: an index of drug defluorination in vivo. Anesthesiology. 1973; 38 (4): 345-51.
32. Magata, Y.; Lang, L. X.; Kiesewetter, D. O., et al., Biologically stable F-18 -labeled benzylfluoride derivatives. Nucl Med Biol. 2000; 27 (2): 163-168.
33. Bonasera, T. A.; Oneil, J. P.; Xu, M., et al., Preclinical evaluation of fluorine-18-labeled androgen receptor ligands in baboons. J Nucl Med. 1996; 37 (6): 1009-1015.

Scheme

Scheme 1 is only available as a download in the Supplemental Files section.

Figures

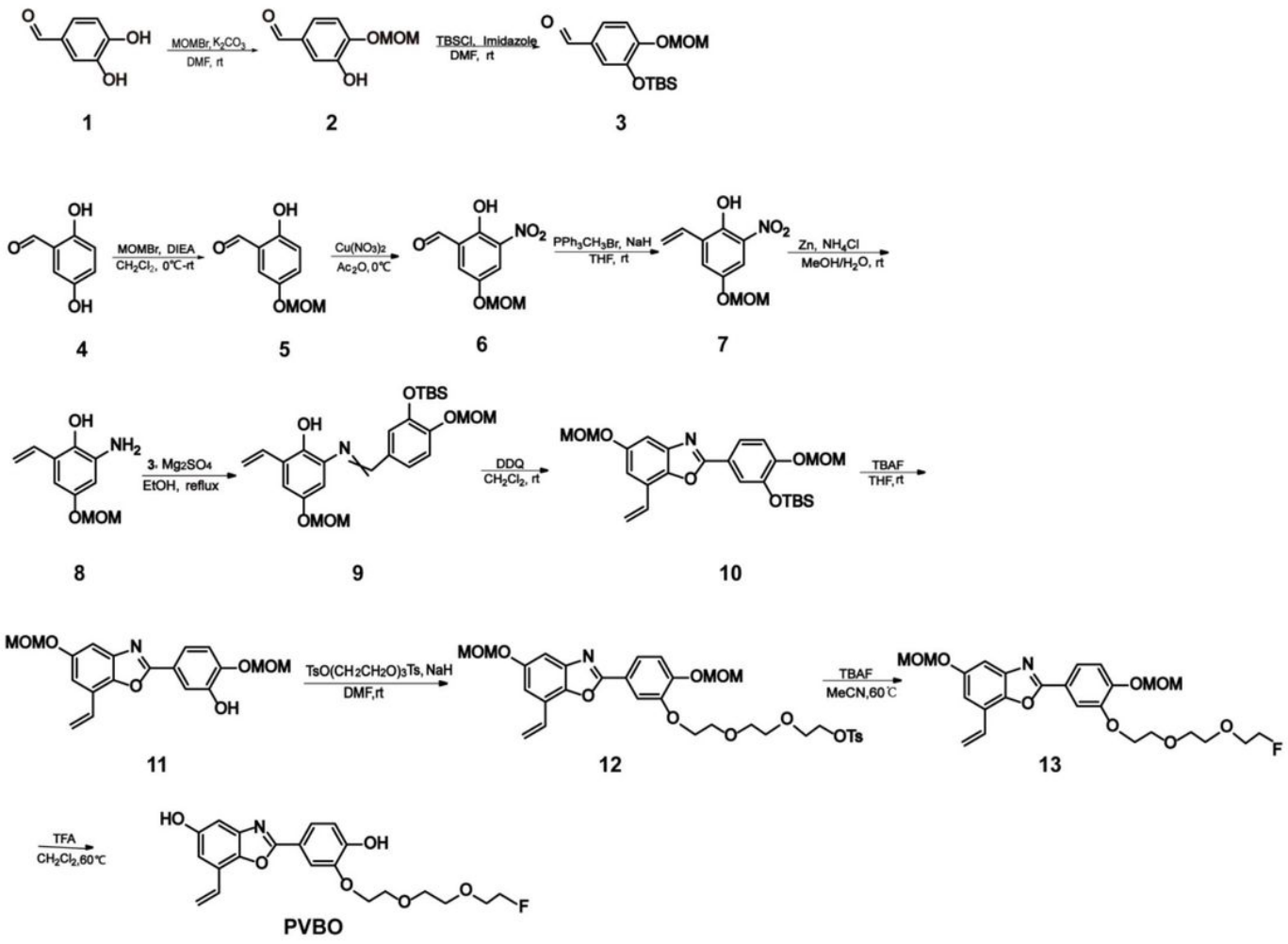

Fig. 1

Figure 1

Synthetic scheme of PVBO

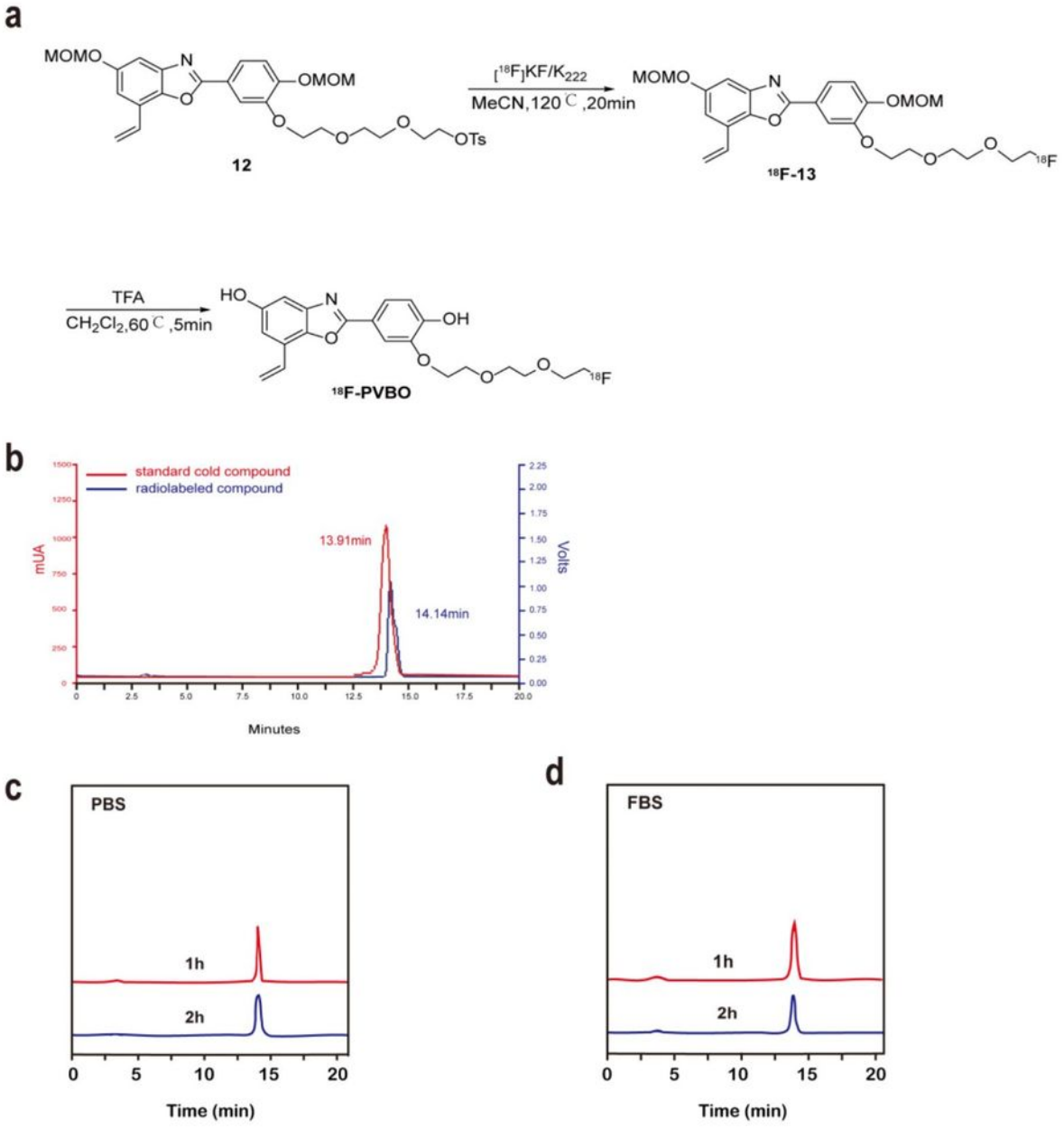

Fig. 2

Figure 2

Radiosynthesis of ^{18}F-PVBO by two-steps radiolabeling (a) Radiosynthetic route of ^{18}F-PVBO. (b) HPLC chromatogram of standard PVBO and ^{18}F-PVBO. Stability analysis of ^{18}F-PVBO incubated with pH = 7.4 PBS (c) and FBS (d) at 37 °C for 1 h and 2 h

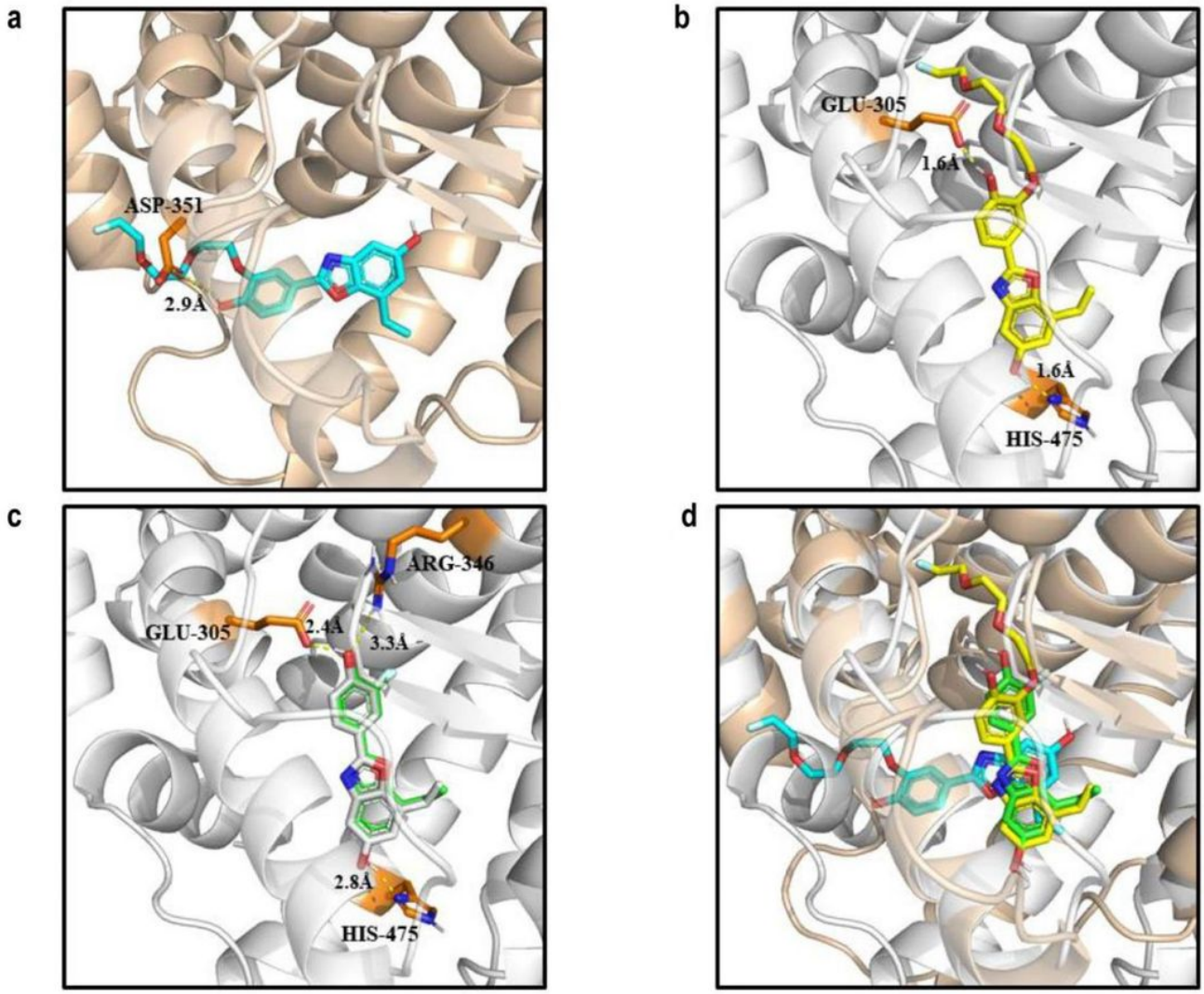

Fig. 3

Figure 3

The docking results of ERα and ERβ. (a) Docking mode of PVBO against ERα [Protein Data Bank (PDB) entry 6VIG], ERα in wheat cartoon, PVBO in cyan sticks. (b) Docking mode of PVBO against ERβ (PDB entry 1X7B), ERβ in gray cartoon, PVBO in yellow sticks. (c) Docking mode of ERB-041 align with the crystal conformation in ERβ (PDB entry 1X7B), ERβ in gray cartoon, ERB-041 crystal conformation in gray sticks, ERB-041 docking pose in green sticks. (d) The superimposition of the docking poses in ERα (PDB entry 6VIG, wheat) and ERβ (PDB entry 1X7B, white). The essential residues are shown in orange sticks,

the polar interactions between the ligands and proteins are shown in yellow dashes and the distance are shown in Å

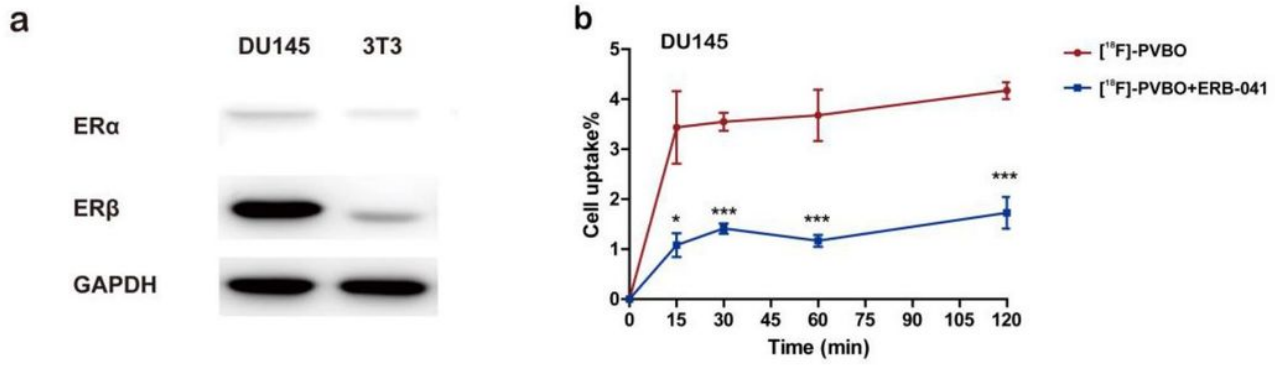

Fig. 4

Figure 4

ER expression in DU145 cells and cell uptake of ^{18}F-PVBO. (a) Western blot analysis of ERα and ERβ in DU145 and 3T3 cells. (b) *In vitro* uptake of ^{18}F-PVBO in DU145 cells in the presence and absence of the ERβ selective drug ERB-041 (*$p < 0.05$; ** $p < 0.01$; *** $p < 0.001$)

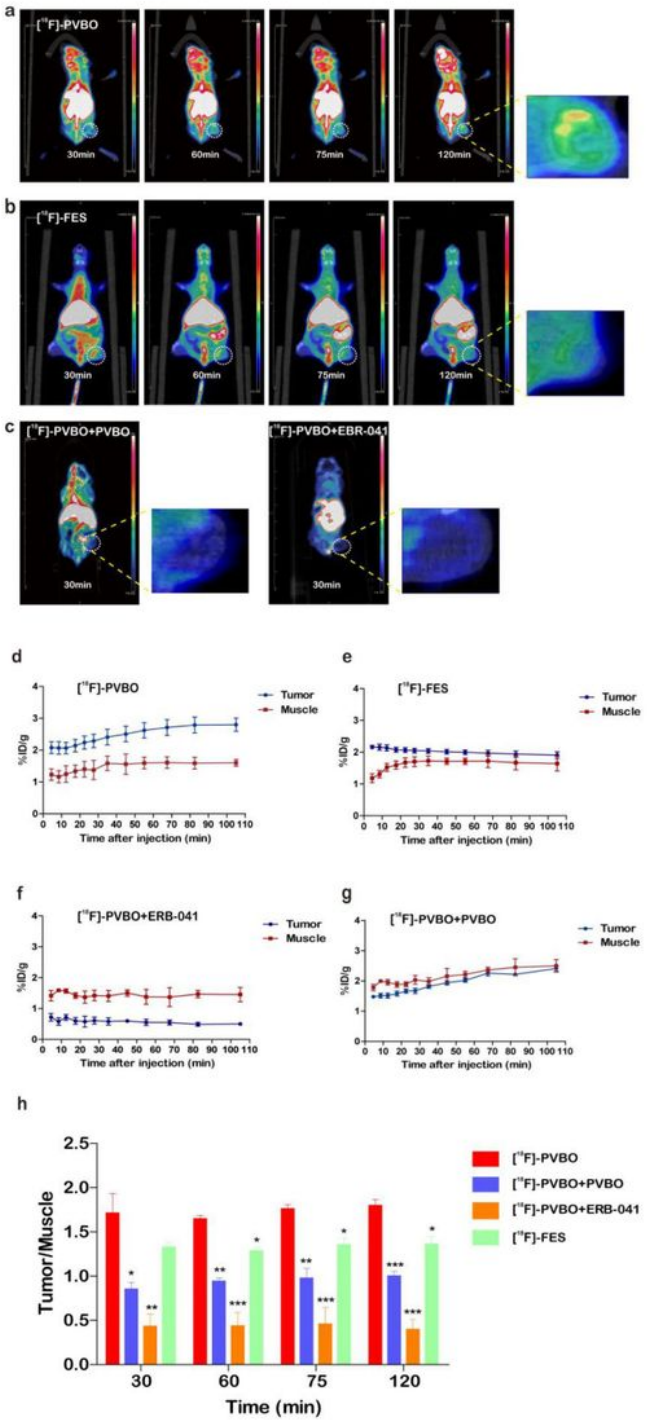

Fig. 5

Figure 5

Representative PET imaging of DU145 tumor-bearing mice at different time points (30, 60, 75 and 120 min) after injection of ^{18}F-PVBO (a), ^{18}F-FES (b), ^{18}F-PVBO pre-injected with PVBO or ERB-041 (c). Tumors were indicated by a white dotted circle. TAC of tumor and muscle uptake from quantitative PET imaging analysis ^{18}F-PVBO (d), ^{18}F-FES (e), ^{18}F-PVBO pre-injected with PVBO (f) and ^{18}F-PVBO pre-injected with ERB-041 (g). (h) Tumor-to-muscle (T/M) ratios (*$p < 0.05$; ** $p < 0.01$; *** $p < 0.001$)

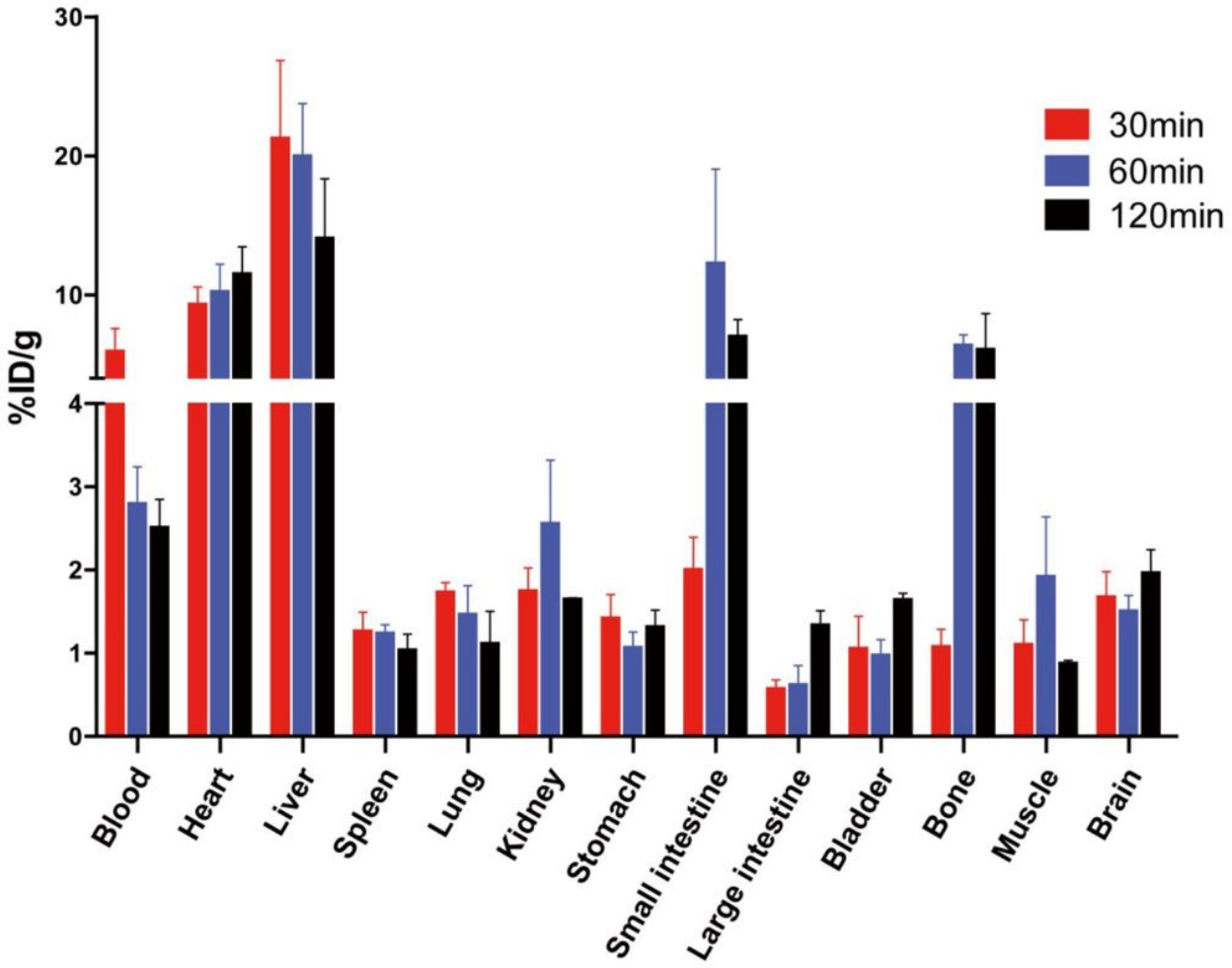

Fig. 6

Figure 6

Biodistribution of ^{18}F-PVBO at 30, 60, 120 min post-injection in BALB/c mice (n = 5 per group)

Supplementary Files

This is a list of supplementary files associated with this preprint. Click to download.

- Scheme1.jpg
- SupplementmaterialEJNMMI.docx